Article

Recognizing the Binding Pattern and Dissociation Pathways of the p300 Taz2-p53 TAD2 Complex

Tongtong Li, Stefano Motta,* Amy O. Stevens, Shenghan Song, Emily Hendrix, Alessandro Pandini, and Yi He*

ACCESS | 📊 Metrics & More | 📖 Article Recommendations | 🗎 Supporting Information

ABSTRACT: The dynamic association and dissociation between proteins are the basis of cellular signal transduction. This process becomes much more complicated if one or both interaction partners are intrinsically disordered because intrinsically disordered proteins can undergo disorder-to-order transitions upon binding to their partners. p53, a transcription factor with disordered regions, plays significant roles in many cellular signaling pathways. It is critical to understand the binding/unbinding mechanism involving these disordered regions of p53 at the residue level to reveal how p53 performs its biological functions. Here, we studied the dissociation process of the intrinsically disordered N-terminal transactivation domain 2 (TAD2) of p53 and the transcriptional adaptor zinc-binding 2 (Taz2) domain of transcriptional coactivator p300 using a combination of classical molecular dynamics, steered molecular dynamics, self-organizing maps, and time-resolved force distribution analysis (TRFDA). We observed two different dissociation pathways with different probabilities. One dissociation pathway starts from the TAD2 N-terminus and propagates to the α-helix and finally the C-terminus. The other dissociation pathway is in the opposite order. Subsequent TRFDA results reveal that key residues in TAD2 play critical roles. Besides the residues in agreement with previous experimental results, we also highlighted some other residues that play important roles in the disassociation process. In the dissociation process, non-native interactions were formed to partially compensate for the energy loss due to the breaking of surrounding native interactions. Moreover, our statistical analysis results of other experimentally determined complex structures involving either Taz2 or TAD2 suggest that the binding of the Taz2-TAD2 complex is mainly governed by the binding site of Taz2, which includes three main binding regions. Therefore, the complexes involving Taz2 may follow similar binding/unbinding behaviors, which could be studied together to generate common principles.

KEYWORDS: dissociation pathway, p53 TAD2, p300 Taz2, steered molecular dynamics (SMD), self-organizing maps (SOMs), time-resolved force distribution analysis (TRFDA), machine learning
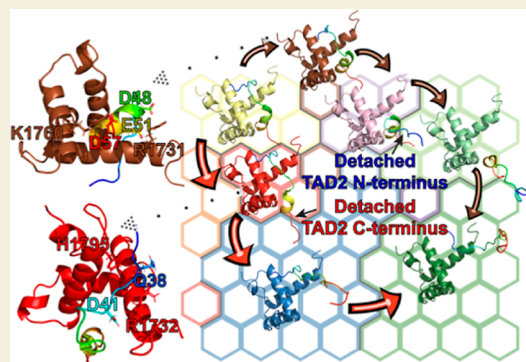
INTRODUCTION

p53 is a tumor suppressor that regulates various essential cellular activities, such as cell period, apoptosis, and gene stability.[1] Dysfunction of p53 was suggested to be associated with different types of cancers.[2−4] In normal cells, p53 can be degraded after being labeled with ubiquitin by murine double minute 2 (MDM2)[5] and can be activated and accumulated by stimulation of various stress signals.[6] The activated p53 subsequently mediates the transcription of downstream genes, such as p21 and bax, which are involved in cell-cycle arrest and apoptosis.[7,8] Previous reports demonstrated that the histone acetyltransferase p300 or its paralog CREB-binding protein (CBP) cofactors play an essential role in the cell-cycle and apoptosis signaling pathways of p53.[9,10] In addition, the interaction between the CBP transcriptional adaptor zinc-binding 2 (Taz2) domain and nucleosomal DNA, specifically acetylating histone H3 lysine 27 (H3K27), is essential for activating the enhancers and promoters of target genes.[11]

Similarly, p53, classified as the pioneer transcription factor, can also directly bind with nucleosomal DNA via the interaction between the N-terminal region (amino acid 1−93) and the histone H3−H4.[12] Therefore, designing chemotherapy drugs targeting CBP/p300 cofactors or p53 is a potential strategy in cancer therapy. For example, EGCG[5] is a small molecule isolated from green tea, which has gained attention as a potential cancer drug because it binds to the disordered N-terminal domain (NTD) of p53 and disrupts the interactions between p53 and MDM2. A recent study demonstrated that the N-terminal transactivation domain 2 (TAD2) and the
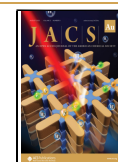
proline-rich region of p53 increased the interaction specificity between the p53 DNA binding domain (DBD) and DNA by binding dynamically at or near the DNA binding site.[13] Specifically, two cancer mutation hotspots in DBD were identified which could form interactions with TAD2.[13]

Over the past few years, many efforts have been put toward exploring the complex between p300 and p53. Some pioneering studies have revealed that p53 can form a homo-tetramer, which binds with p300 through interactions of p53 TAD and the four domains of p300 (Taz1, Kix, Taz2, and IBiD).[14,15] Among the four domains, Taz2 forms the tightest contact with TAD.[15] An NMR study indicated that Taz2 is composed of four helices: $\alpha1$, $\alpha2$, $\alpha3$, and $\alpha4$.[16] The intrinsically disordered TAD of p53 contains two subdomains, TAD1 and TAD2, both of which can bind with Taz2 of p300.[16] The transient α-helix in isolated TAD2 can be stabilized by embedding itself into the hydrophobic interface formed by helices $\alpha1$, $\alpha2$, and $\alpha3$, in Taz2.[16] Taz2 can form a more stable complex with TAD2 than TAD1 possibly due to more negatively charged residues in TAD2, which complement the positively charged residues at the periphery of the Taz2 binding pocket.[17] Many efforts have been devoted to the study of TAD1,[18−20] while fewer efforts have been focused on TAD2. Furthermore, although some studies have determined the dynamic conformations of TAD2 in the bound states,[15,16] reports about the binding/unbinding mechanism of TAD2 and Taz2 at an atomic resolution are very scarce.

Although both p300 and p53 undertake essential biological functions, the intrinsically disordered nature of p53 TAD2 makes it difficult to uncover the mechanism behind it. Here, we focus on investigating the binding mode and dissociation pathways between p300 Taz2 and p53 TAD2 using a combination of computational techniques, including classical molecular dynamics (MD), steered molecular dynamics (SMD), self-organizing maps (SOMs), and time-resolved force distribution analysis (TRFDA). With such a computational pipeline, we found that the binding between p300 Taz2 and p53 TAD2 enhances the stability of the short helical region near the C-terminus of p53 TAD2. Furthermore, two unique dissociation pathways were identified. Pathway 1 is characterized by the detachment of the p53 TAD2 N-terminus, followed by the detachment of the p53 TAD2 α-helix and C-terminus. In contrast, pathway 2 is characterized by a dissociation process along the inverse direction. Although the detachment sequence of p53 TAD2 in the two pathways was different, both pathways went through neurons (structural states), with high pulling forces identified by SOMs. In order to reveal the residues and interactions that were related to these high pulling forces, TRFDA was used to explore the residue−residue interactions within the p300 Taz2-p53 TAD2 complex, resisting the external pulling forces during the dissociation process and to highlight key residues that play essential roles in each pathway. TRFDA results demonstrated that unique, long-lasting electrostatic interactions exist in each of the two pathways. Root-mean-square deviation (RMSD), solvent accessible surface area (SASA), and the helical fraction of the TAD2 α-helix were traced along the dissociation pathway to demonstrate that the disappearance of the TAD2 α-helix is accompanied by the increment of SASA of the α-helix. The unfolding of the α-helix in the p53 TAD2 and the unbinding of the p300 Taz2-p53 TAD2 complex occur at the same time. During the dissociation process, non-native contacts were created dynamically, especially after the

disruption of surrounding native contacts, which might play an important role in the binding/unbinding process of the p300 Taz2-p53 TAD2 complex. By comparing the p300 Taz2-p53 TAD2 complex with other complexes involving p300 Taz2 or p53 TAD2, the statistical results suggest that the binding of the Taz2-TAD2 complex may be determined by the structure of p300 Taz2. Taken together, this study of the p300 Taz2-p53 TAD2 complex not only provides a better understanding of the possible unbinding mechanism of the p300 Taz2-p53 TAD2 complex but also identifies the binding pattern between p300 Taz2 and p53 TAD2. Such a binding pattern could shed light on future investigations of binding processes between structured proteins and IDPs.

■ METHODS

Classical all-atom molecular dynamics (MD) simulations were carried out for two systems: (1) the p53 TAD2 monomer (extracted from PDB ID: 2MZD[16]) and (2) the p300 Taz2-p53 TAD2 complex (PDB ID: 2MZD[16]) in order to analyze the dynamic information and the helical stability of TAD2 in the bound state and in the isolated state. The combined simulation time is 18 μs.

SMD simulations were carried out to investigate the unbinding behavior of the p300 Taz2-p53 TAD2 complex (PDB ID: 2MZD[16]) by applying a harmonic force on Taz2 and TAD2 and maintaining positional restraints on Taz2. 50 independent SMD simulations were carried out to explore the unbinding process between p300 Taz2 and p53 TAD2. Both MD and SMD simulations were carried out using the CHARMM36m force field.[21]

PathDetect-SOM,[22,23] a tool based on SOMs,[24−26] was used to extract structural patterns from the large number of unbinding events recorded in the simulations. SOMs are a type of unsupervised artificial neural network with an explicit visual representation of data on a two-dimensional map. In this work, the intermolecular distances between the Cβ atoms of p300 Taz2 and p53 TAD2 were used to train the SOMs. The training was performed over 5000 cycles. Furthermore, TRFDA,[27] which provides forces at the atomic resolution and punctual stress at the residue resolution, was performed to trace key residues in the dissociation process.

The experimental structures of eight complexes involving Taz2 and TAD from different proteins (p53 TAD2-2MZD,[16] p53 TAD1-2K8F,[19] STAT1 TAD-2KA6,[28] E1A-2KJE,[29] p53 TAD2-5HP0,[30] p53 TAD-5HPD,[30] p63 TAD-6FGN,[31] and p73 TAD1-6FGS[31]) were analyzed using contact maps in order to capture the common binding pattern among the complexes.

More details of simulation setup and data analysis methods and parameters are available in the Supporting Information.

■ RESULTS

Structural and Dynamical Differences of p53 TAD2 in Isolation and in Complex

Classical MD simulations of isolated p53 TAD2 and the p300 Taz2-p53 TAD2 complex reveal that the p53 TAD2 α-helix (residues 47−55) was stable only in the complex state, but the terminal regions, especially the p53 TAD2 N-terminus, remain dynamic even in the Taz2-TAD2 complex. These results are consistent with the finding of the fuzzy p53 NTD in complex with EGCG.[5] More details can be found in section "changes in structures and dynamics of p53 TAD2 in isolation and in complex" in the Supporting Information. Such results also agree with previous work.[32]

Dissociation can Start at Either the N- or C- Terminus of p53 TAD2

To investigate the unbinding process which can give insights into the unbinding mechanisms, 50 replicas of SMD simulations were carried out to provide sufficient dissociation
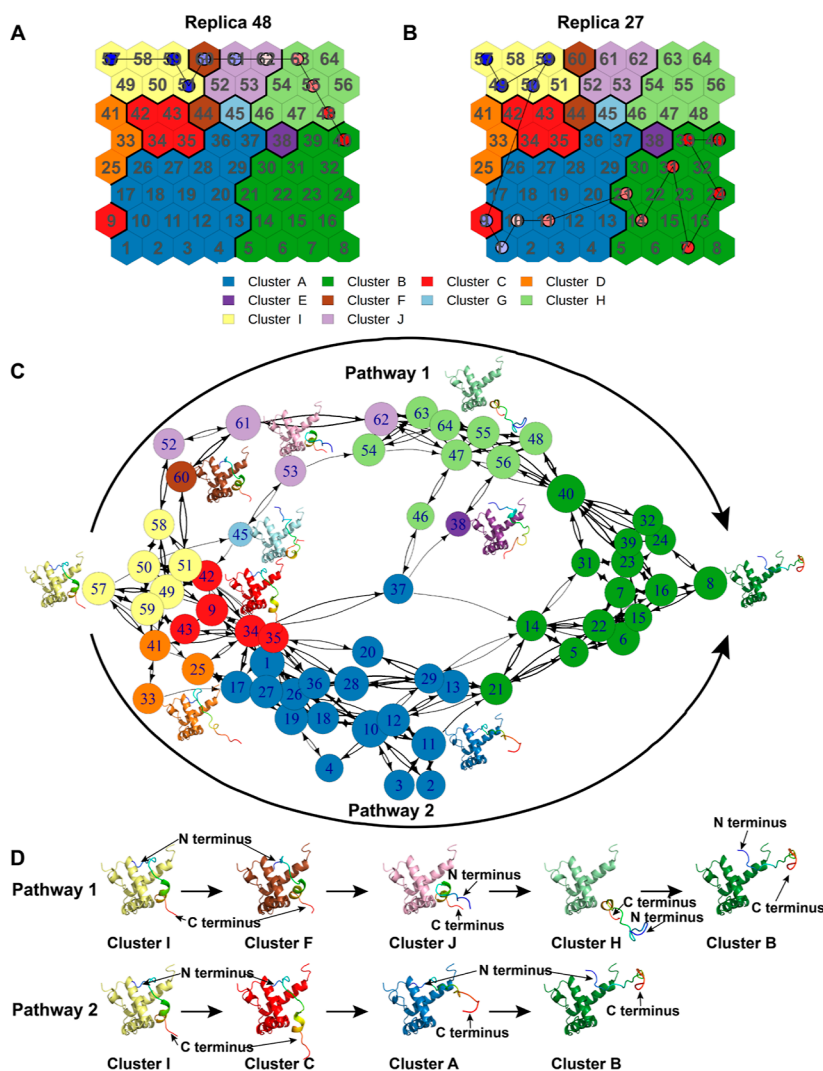
Figure 1. Two pathways were determined with SOMs, replicas 48 (A) and 27 (B) representing pathways 1 and 2, respectively. The neuron numbers are labeled on the map. (C) Diagram of the transition matrix between neurons. The representative structure for each cluster was displayed beside the corresponding cluster with Taz2 colored in the same way as the clusters. (D) Cartoon structures covered for the typical pathways 1 and 2 are displayed. Pathway 1 started from cluster I, usually went through clusters F, J, and H, and ended at cluster B, while pathway 2 usually went through clusters C and A instead. Taz2 in the clusters are colored with the same code as panel A. TAD2 is colored in rainbow from the N-terminus (blue) to C-terminus (red) with the N/C-terminus labeled by the side of TAD2.

events of the Taz2-TAD2 complex. A common pattern during unbinding transitions was identified using SOMs, which can help recover the unbinding events in a low dimensional representation and then identify the dissociation pathways.

The distances between $C\beta$ atoms of Taz2 and TAD2 residues were used as input to train a SOM of 8×8 neurons. For each conformation, distances are presented as a vector of values, and neuron weights are iteratively updated to model the input space (Supporting Information). At the end of the training, a neuron describes a group of conformations with very similar input vectors so that it approximates a microstate. Similar neurons are further grouped into clusters, with the goal of identifying possible macrostates. The 64 neurons were grouped into 10 clusters (A–J), the top left and bottom right clusters denoting the native and dissociated Taz2-TAD2 complex, respectively, as shown in Figure S2 of the Supporting Information. The representative structure for each neuron was mapped on the trained SOM, illustrating the bound status at each neuron (Figure S3). By tracing the pathways followed by

each replica on the SOM (Figures S4 and S5), common patterns can be identified for the unbinding process. The two representative unbinding pathways are shown in Figure 1A,B, where the two replicas went through different clusters and exemplified pathways 1 and 2, respectively.

Using a transition matrix obtained from SOMs, a network model was constructed to demonstrate the two dissociation pathways (Figure 1C). Most replicas in pathway 1, started from cluster I (the native structure, on the left), went through clusters F, J, and H, (on top of the network), and ended at cluster B (the dissociated structure, on the right). In this pathway, the unbinding was initiated at the TAD2 N-terminus, followed by the detachment of the α-helix and finally the C-terminus. In contrast, most replicas in pathway 2 went through clusters C and A (at the bottom of the network) instead of clusters F, J, and H. In pathway 2, the dissociation order was completely opposite, starting from the C-terminus of p53 TAD2. Because the C-terminus is associated with the rigid α-helix of TAD2, once the C-terminus had departed from Taz2,
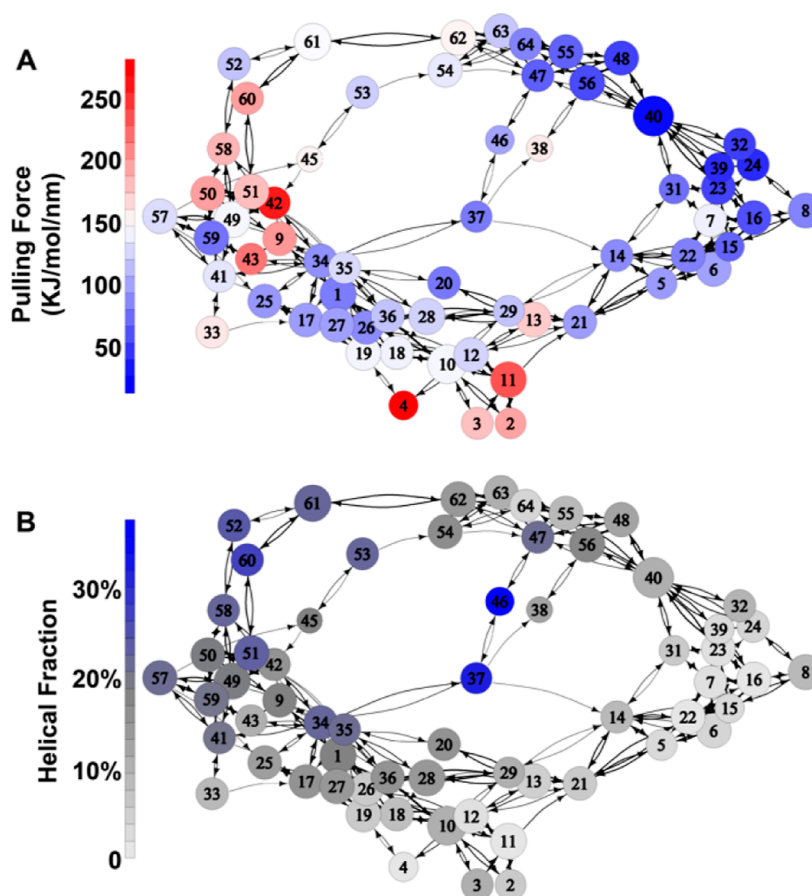
Figure 2. Average pulling forces (A) and the helical fractions of TAD2 (B) mapped on the SOM. Neurons are labeled with neuron indexes. In panel B, the helical fraction is in the range of 0−100%, with 0 denoting that there is no helical structure and 100% denoting all residues forming the helical structure.

the α-helix dissociated successively. Finally, the detachment of the N-terminus followed. The representative structures for the two pathways are shown in Figure 1D. In a few simulations, the dissociation passes through neuron 37 to bridge pathways 1 and 2 (replicas 22 and 43 in Figure S4). In these simulations, the unbinding started from the C-terminus, but continued with the unbinding of the N-terminus, leaving only the rigid α-helix of p53 TAD2 bound to Taz2.

To identify the correlations between the pulling force and the pathways, the pulling forces of each SMD trajectory were mapped to the SOM, and then the average pulling force of each neuron was calculated over all the frames assigned to that neuron (Figures 2A and S6A). In both pathways, we identified neurons associated to high forces (such as 51, 58, and 60 in pathway 1 and 42 and 43 in pathway 2). In both cases, maximum forces were associated with transitions in the first part of the pathways, indicating that starting of the unbinding from either the C-terminus or N-terminus is the key step for the mechanism. As the unbinding continues, simulations following pathway 1 proceed without a significant peak in the forces, while simulations following pathway 2 need to overcome another energetic barrier in correspondence of neurons 2, 3, 4, and 11. These neurons were sampled only by a small subset of replicas, indicating that this barrier may be circumvented. It was suggested that the helix near the C-terminus of p53 TAD2 plays a significant role to stabilize the p53 TAD2 and p300 Taz2 complex.[16] For this reason, in addition to mapping pulling forces, the helical fractions of p53

TAD2 during the pulling process were also mapped to the SOM to trace the unfolding of TAD2 along pathways 1 and 2. As shown in Figures 2B and S6B, the helical contents were different for the two pathways. The neurons at the beginning of pathway 1 were able to maintain the α-helix (helical fraction of clusters I, F, and J above 20%), while the helical fraction dropped quickly in pathway 2 after entering cluster A. In some cases, the broken helix can be reformed, as observed in neurons 37 and 46 (Figures 2B and S6B). When the helical fraction analysis results were considered together with the pulling force analysis, the high pulling forces of neurons 58, 51, and 60 were expected to be related to the disruption of interactions between Taz2 and TAD2, given the relatively high helical fraction (Figures 2 and S7A,F). On the other side, the high forces of neurons 42, 43, and 9 were expected to be related to the partial destruction of the TAD2 helix, considering the low helical fractions, and the disruption of interactions between Taz2 and TAD2 (Figures 2 and S7D,I). According to this analysis, pathway 2 shows elements consistent with an induced fit mechanism, given that the folded helical structure is lost at the very beginning of the process. In pathway 1, the structure of TAD2 is preserved even in the later stages of the process (Figure S8).

Unbinding Process was Accompanied by the Unfolding of the p53 TAD2 α-Helix

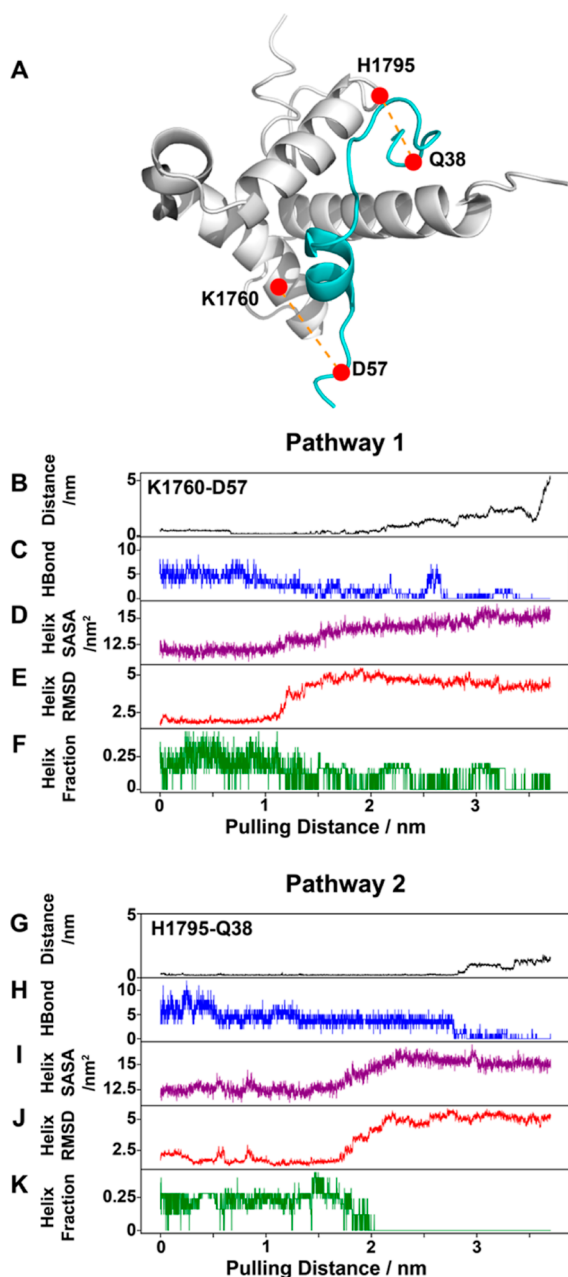As shown in Figure 3, the separation of p300 Taz2 and p53 TAD2 is accompanied by the unfolding of the p53 TAD2 α-

Figure 3. Unfolding of the TAD2 α-helix and the unbinding process of the complex. Panels (B−F) and (G−K) are for pathway 1 (replica 48) and pathway 2 (replica 27), respectively. For each pathway, the distance of key residue pairs [(B,G) the residue pairs are labeled in panel (A), Taz2 K1760-TAD2 D57 for pathway 1, and Taz2 H1795-TAD2 Q38 for pathway 2], the number of hydrogen bonds (C,H), SASA of the TAD2 α-helix (D,I), RMSD of the TAD2 α-helix (E,J) with the TAD2 α-helix in the experimentally determined complex as the reference, and the helical fraction of TAD2 (F,I) was obtained to illustrate the unbinding process.

helix. The applied pulling force resulted in an increased distance between key residue pairs (Figure 3B,G) and fewer hydrogen bonds between TAD2 and Taz2 (Figure 3C,H). The departure of key residue pairs (Figure 3A,B,G) suggested that the unbinding process had almost reached the end. As the Taz2-TAD2 complex pulls apart, the buried hydrophobic interface is gradually exposed to the solvent, giving rise to the increase in the total solvent accessible surface area (SASA). For example, the SASA of the TAD2 α-helix (residues 47−55)

increases from 12 to 15 nm^2 (Figure 3D,I). Both the dissociation between p300 Taz2 and p53 TAD2 and the order-to-disorder transition of the p53 TAD2 α-helix occurred simultaneously, which was evaluated by the RMSD with the TAD2 α-helix in the native Taz2-TAD2 complex as the reference and the helical fraction of TAD2 (Figure 3E,F,J,K). The RMSD (Figure 3E,J) increased, and at the same time, the SASA of the TAD2 α-helix increased as well (Figure 3D,I). To visualize the variation of the secondary structure of TAD2 with SASA more clearly, the SASA profile was overlapped with the secondary structure plots of TAD2 (Figure S9), which suggested that the hydrophobic core involving residues W53 and F54 in the α-helix in TAD2 contributed to the stabilization of the complex. This is understandable when TAD2 leaves Taz2 and loses some of its interactions and the hydrophobic core with Taz2, causing the increment of SASA in the TAD2 helix, it becomes difficult to maintain the helical structure. The structural transition of the TAD2 α-helix (Figure 3E,F,J,K) happened earlier than the detachment of the TAD2 C-terminus in pathway 1 (Figure 3B, the distance of K1760-D57, which was identified as critical residue pairs by the TRFDA results in the next section, could be used to indicate the detachment of the TAD2 C-terminus) and the detachment of TAD2 N-terminus in pathway 2 (Figure 3G, the distance of H1795-Q38 indicating the detachment of the TAD2 N-terminus), which was consistent with the SOMs results. Results for every trajectory are shown in Figures S10 and S11 in the Supporting Information. Analyses shown in Figure 3 were done using MDTraj[33] and the Bio3D packages.[34−37]

The helical fraction of p53 TAD2 decreased as the unbinding process of the complex proceeds. Furthermore, the unfolding process varied for different pathways. One of the key questions that needs to be addressed is what residues and physical interactions determine the disassociation process. To identify the key residues and physical interactions regulating the two unique pathways, TRFDA and further analyses were performed to identify the critical residues and interactions in the disassociation process of the p300 Taz2-p53 TAD2 complex.

Critical Residues and Interactions along the Two Pathways

TRFDA between p300 Taz2 and p53 TAD2 was performed for each SMD trajectory to evaluate the evolution of the punctual stress at each residue, which were averaged every 40 frames, along the dissociation process. TRFDA can trace punctual stress acting on any residue of interest so that it can be used to assess the forces acting on the residues and their resistance against external perturbations. To avoid bias to a particular trajectory, Figure 4A,B corresponds to the average punctual stress of p53 TAD2 in pathways 1 and 2, respectively. From the perspective of punctual stress on p53 TAD2, the TRFDA results clearly suggest that the p53 TAD2 N-terminus resisted against the pulling force in pathway 2 (Figure 4B) and thus significantly contributed to maintaining the stability of the complex. Oppositely, in pathway 1 (Figure 4A), the punctual stress on the p53 TAD2 C-terminus residues were stronger and more continuous. More interestingly, the residues that played critical roles in the native complex (e.g., residue E56) undertook large stresses at the initial stage of the pulling process but did not significantly contribute to either pathway. Instead, the punctual stress on residue D57 at the C-terminus in pathway 1 and residues at the N-terminus in pathway 2 increased gradually, and ultimately, these stresses are what
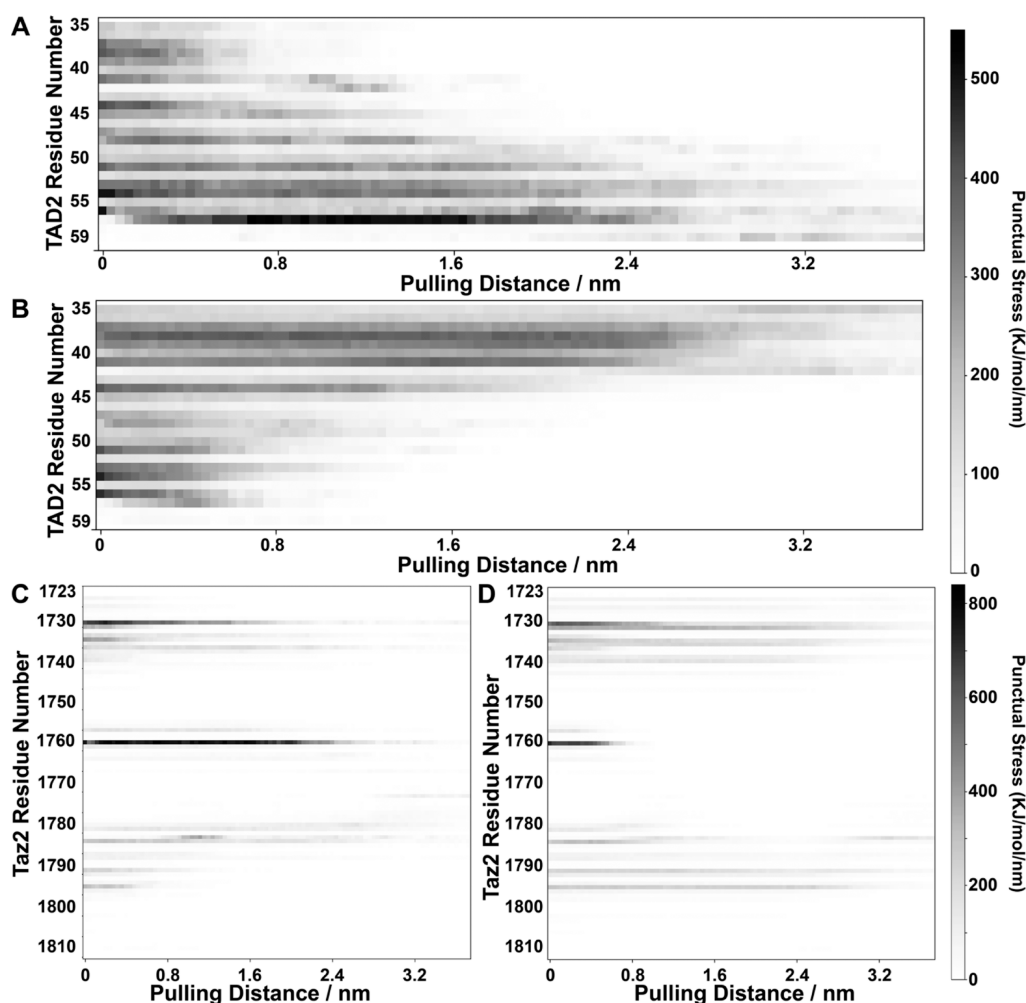
Figure 4. Punctual stress on TAD2, averaged over 14 SMD replicas [pathway 1 (A)] and 36 SMD replicas [pathway 2 (B)]. The punctual stress on Taz2, averaged over 14 SMD replicas [pathway 1 (C)] and 36 SMD replicas [pathway 2 (D)].

determined the pathways. From the perspective of punctual stress on p300 Taz2, residue K1760 in pathway 1 (Figure 4C) and residues in the range of p300 Taz2 1731−1740 and 1791−1795 in pathway 2 (Figure 4D) were significant contributors.

In order to uncover the dissociation mechanism in detail, we need to capture the critical residue pairs in the dissociation process and monitor their contributions along the two pathways. Several residues of p300 Taz2 with high punctual stress in each pathway were selected to identify their interactions with the entire p53 TAD2 (Table S1). These critical residues in pathways 1 (Figure 5A,B) and 2 (Figure 5C) were displayed in the complex. As shown in Figure 4C, punctual stress on residues p300 Taz2 K1760 and R1731 was critical for pathway 1; therefore, these two residues were selected to perform per residue TRFDA between the single residue and p53 TAD2. As shown in Figure 5D,E, the pairwise interactions of p300 Taz2 K1760-TAD2 D57, p300 Taz2 R1731-p53 TAD2 D48, and p300 Taz2 R1731-p53 TAD2 E51 play critical roles in pathway 1. In pathway 2, p300 Taz2 residues H1795 and R1732 were selected to perform per residue TRFDA to identify critical pairwise interactions, which include p300 Taz2 H1795-p53 TAD2 Q38 (Figure 5F), Taz2 R1732-TAD2 Q38, and Taz2 R1732-TAD2 D41 (Figure 5G). The initial punctual stress on these key residue pairs is stronger than that of the Taz2 residue with the remaining TAD2

residues, indicating that these electrostatic interactions significantly contribute to the initial stability of the complex, which is confirmed by NMR results.[16] Importantly, most of the key residue pairs shown in Table S1 are native contacts identified in the same experimental work.[16] For example, NMR results highlight R1731-D48, R1732-D41, R1737-E51, and I1781−W53 as key interactions in the complex.[16] Some other interactions were also determined as native contacts, including R1731-E51, R1731-D41, R1732-Q38, S1734-E51, I1735-M44, and H1795-Q38. Notably, their contribution, specifically R1731-D48 and R1732-Q38, becomes more obvious as the dissociation progresses, as observed in Figure 5E,G. For example, the pairwise interaction between p300 Taz2 K1760 and p53 TAD2 D57 was initially absent but quickly appeared as the pulling simulation progressed (Figure 5D). This change in punctual stress can be explained by the native interaction between p300 Taz2 K1760 and p53 TAD2 E56 shifting to D57 after the pulling force was applied. It is worth noting that the key residue pairs are charged residues; thus, electrostatic interactions may play critical roles in the unbinding process. Additional residues of p300 Taz2 and p53 TAD2 were selected to conduct similar analyses, and the corresponding figures can be found in Figures S12−S14. In addition to electrostatic interactions, some hydrophobic interactions also significantly contribute to the dissociation process, such as p300 Taz2
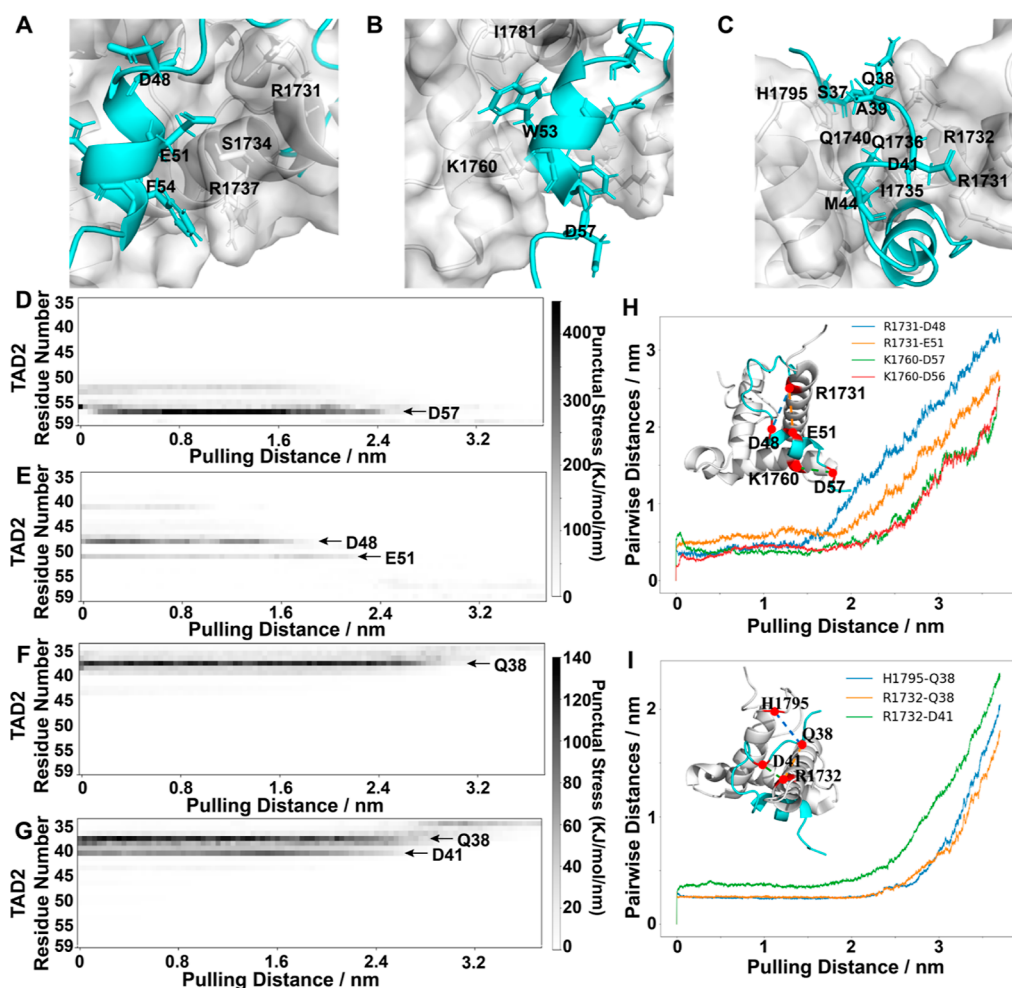
Figure 5. Critical residues in pathway 1 (A,B) and pathway 2 (C). Critical residues of Taz2 in the dissociation pathway (D−G) and the corresponding pairwise distance change along the dissociation process (H,I). D−G stands for the interactions between the selected Taz2 residue with the entire TAD2 to identify the critical interactions between the selected Taz2 residue with TAD2 residues. (D,E) are the punctual stress between Taz2 K1760 and R1731 with TAD2, respectively. (F,G) are the punctual stress between Taz2 H1795 and R1732 with TAD2, respectively. In panel (H), the distance between Taz2 K1760 and TAD2 D56 is also shown to illustrate the native contact shifting from TAD2 D56 to TAD2 D57. Panels (D,E,H) correspond to pathway 1, while panels (F,G,I) correspond to pathway 2.

I1781-p53 TAD2 W53 in pathway 1 and p300 Taz2 I1735-p53 TAD2 M44 in pathway 2. Next, the distances of the key residue pairs mentioned above were monitored along the dissociation pathway (Figure 5H,I), suggesting that these pairwise residues considerably resist the external pulling force. Additionally, the distance between Taz2 K1760 and TAD2 D56 is also shown in Figure 5H. The distance immediately increases after the application of the external force, indicating the rupture of the native contact. Once Taz2 K1760 establishes interaction with TAD2 D57, the distance between Taz2 K1760 and TAD2 D56 decreases due to the physical position between D56 and D57.

Binding Pattern of the Taz2-TAD2 Complex

Eight complexes involving Taz2 [Taz2-p53 TAD2 (PDB ID, 2MZD[16]), Taz2-p53 TAD2 (PDB ID, 5HP0[30]), Taz2-p53 TAD (PDB ID, 5HPD[30]), Taz2-p53 TAD1 (PDB ID, 2K8F[19]), Taz2-p63 TAD (PDB ID, 6FGN[31]), Taz2-p73 TAD1 (PDB ID, 6FGS[31]), Taz2-STAT1 TAD (PDB ID, 2KA6[28]), and Taz2-E1A (PDB ID, 2KJE[29])], as shown in Figure 6C−J, were selected to investigate the binding pattern between p300 Taz2 and p53 TAD2 with contact map analysis. Their contact maps were found to follow similar binding patterns. Taking the Taz2-TAD2 complex as an example (Figure 6A), there were three main regions in Taz2, forming interactions with TAD2, including the N-terminus, the middle region, and the C-terminus. The middle region of Taz2 formed contacts mainly with the TAD2 C-terminus. The Taz2 terminal regions formed contacts mainly with the TAD2 α-helix and the N-terminus. For example, Taz2 residues R1731, R1732, S1734, I1735, Q1736, R1737, and Q1740 are located in the N-terminus region, K1760 is located in the middle region, and I1781 and H1795 are located in the C-terminus region (Table S1). This binding pocket was common in the eight complexes involving Taz2 (Figure 6B). The average contact maps indicate that TADs form contact with three major regions of Taz2, including the N-terminus, the middle region, and C-terminus, corresponding to α1, α2, and α3 helices, respectively.

Notably, there was a subtle difference among these three regions for the different TADs (Figure S15B). This indicated that the eight TADs mentioned above formed native contacts mainly with the similar interface formed by α1, α2, and α3 helices, but the binding sites varied slightly from case to case. The binding pocket of Taz2 contained most of the hydro-
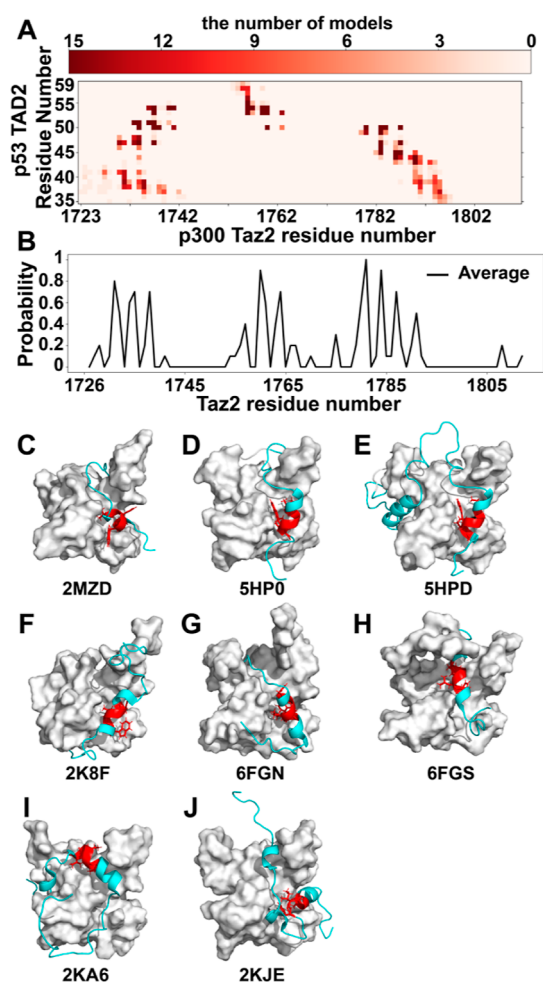
Figure 6. (A) Contact map of the p300 Taz2-p53 TAD2 complex was calculated from the 15 models determined by NMR.[16] The scale bar represents the frequency of contacts at the same residue pair among 15 models, with 0 denoting that there is no contact in any model and 15 denoting contacts in all models. (B) Probability of forming contacts of Taz2 in complex with TADs from different transcriptional factors. (The residue number is labeled according to p300 Taz2, for example, residue 1726 in p300 Taz2 corresponds to residue 1764 in CBP). Taz2 complexes, (C) Taz2-p53 TAD2 (PDB ID, 2MZD[16]), (D) Taz2-p53 TAD2 (PDB ID, 5HP0[30]), (E) Taz2-p53 TAD (PDB ID, 5HPD[30]), (F) Taz2-p53 TAD1 (PDB ID, 2K8F[19]), (G) Taz2-p63 TAD (PDB ID, 6FGN[31]), (H) Taz2-p73 TAD1 (PDB ID, 6FGS[31]), (I) Taz2-STAT1 TAD (PDB ID, 2KA6[28]), and (J) Taz2-E1A (PDB ID, 2KJE[29]).

phobic residues and some positively charged residues at the marginal region, interacting with the acidic amphipathic α-helix in TADs. The stability of these complexes is related to the hydrophobic and electrostatic interactions between Taz2 and TADs. Therefore, the binding/unbinding kinetics of these complexes should be studied together to reveal the general principles followed by these systems.

Taken together, the binding of the p300 Taz2-p53 TAD2 complex was determined by the residue distribution of the binding pocket in Taz2. In the complexes involving Taz2, although the TADs had different sequences, they contained a similar ΦXXΦΦ motif (Figure S15A), where Φ denotes hydrophobic residues and X denotes any type of residue after sequence alignment.[37] Therefore, when binding with Taz2, they adopted a similar canonical helical structure.

DISCUSSION

Dissociation Behavior of the p300 Taz2-p53 TAD2 Complex

The unbinding events crossing high-energy barriers could be accessible via SMD simulations by applying external forces. The unbinding process was further analyzed with SOMs and TRFDA to provide a low dimensional representation of the unbinding process, giving rise to clear dissociation pathways and to determine critical residues in the process. The 50 replicas of SMD trajectories were grouped into two pathways by SOMs, 36 unbinding events occurred in pathway 2, and 14 unbinding events occurred in pathway 1. In pathway 2, the dissociation started from the TAD2 C-terminus, followed by the α-helix and the N-terminus, while in pathway 1, the dissociation sequence was opposite, starting from the N-terminus to the α-helix and finally to the C-terminus. Both unfavorable pathway 1 and favorable pathway 2 had to visit neurons with frames corresponding to high pulling forces, which was illustrated by the pulling force map (Figures 2A and S6A). In order to analyze the contributions of critical residue pairs unique in the two pathways, the punctual stress of Taz2 and TAD2 together with per residue punctual stress was generated to identify the long-lasting interactions during the dissociation process. The TRFDA results demonstrate that the TAD2 N-terminus formed strong interaction networks with Taz2 helices α1 (N-terminal region) and α3 (C-terminal region) (Figure 4B,D). The separation between the TAD2 N-terminus with Taz2 required strong forces (Figure 4B), indicating that the TAD2 N-terminus contributed greatly to the unbinding dynamics of the complex. It is worth noting that the contribution of Taz2 K1760 was obviously different in pathways 1 and 2 (Figure 4C,D). K1760 can form contacts with TAD2 E56 in the native Taz2-TAD2 complex. In pathway 1 (Figure 5D), the K1760-E56 interaction disappeared at the beginning of the dissociation process, and then K1760 quickly formed interaction with the adjacent D57. However, in pathway 2, the interactions between K1760 and D57 also quickly disappeared after shifting from interaction K1760-E56 (Figure S14B). In this way, the connection between Taz2 K1760 and two key residues (E56 and D57) at the TAD2 C-terminus was broken at the beginning of the dissociation process. Additionally, the charged residues in the TAD2 C-terminus are quite dispersed (Figure 5A−C). This might explain why the TAD2 C-terminus in pathway 2 was much easier to depart. In addition, the helical contents of TAD2 in the two pathways differed greatly. For example, the TAD2 α-helix was maintained for a significant period of time in pathway 1 (Figure 2B and S6B). With the separation of Taz2 and TAD2, the hydrophobic interface was exposed to the solvent, leading to an increase of the solvent accessible surface area. Without the immobilization of intermolecular interactions with Taz2, the TAD2 α-helix became more dynamic and was destroyed gradually (as shown in Figure 3).

The pairwise punctual stress provide insights into the recognition kinetics between Taz2 and TAD2. A previous report showed that the fast association rate[17] might be related to the long-range electrostatic potentials and the large capture radius of the disordered region, according to the fly-casting mechanism.[38] TAD2 contains many negatively charged residues and forms an amphipathic helix embedded in the Taz2 binding pocket (as shown in Figure S16A). This is consistent with our per residue punctual stress results which

show that many negatively charged residues in TAD2 play critical roles in the dissociation process. Notably, some native interactions are relatively weak, such as interactions involving TAD2 E56. As shown in Table S1, most key residue pairs identified from TRFDA form hydrophobic and electrostatic interactions, which are consistent with the native contacts observed in the experimental work.[16] It is noted that some dynamic non-native contacts were formed during the dissociation process, such as the interaction between Taz2 K1760 and TAD2 D57 in pathway 1. These non-native contacts may play a role in protein–protein recognition. In the recognition mechanism between Taz2 and TAD2, the electrostatic interactions may accelerate the encounter rate, and TAD2 can rearrange itself to form more native contacts with Taz2. This understanding may further explain the specificity between Taz2 and TAD2.

Binding Mode of Complexes Involving Taz2

By comparing the binding pattern of various Taz2 and TAD2 complexes, the contact map analysis suggests that the binding of Taz2 and TAD2 could be determined mainly by the structure of Taz2. In the PH-TAD2 complex, TAD2 rearranges itself to be an extended string to bind to the PH domain, indicating the plasticity of disordered proteins. However, in the complexes involving Taz2, the TADs from different proteins form a short helix and bind with three main regions in Taz2, including the N-terminus, the middle region, and the C-terminus.

Beside the complexes involving Taz2, two complexes involving p53 TAD2 [Taz2-p53 TAD2 (PDB ID, 2MZD[16]) and PH-p53 TAD2 (PDB ID: 2RUK[39])] were selected to reveal the factors determining the structure of p53 TAD2 in the complex. As shown in Figure S16, compared with the structure of TAD2 in the p300 Taz2-p53 TAD2 complex, p53 TAD2 (phosphorylated at Ser46 and Thr55) interacted with the PH domain of TFIIH p62 in an extended string pattern rather than the canonical amphipathic α-helix.[39] This is because the binding pocket of PH involved seven lysine residues to provide enough degrees of freedom for negatively charged residues in TAD2, and the aromatic ring of TAD2 Trp53 was inserted into the hydrophobic groove of the PH domain to immobilize TAD2 at the binding pocket specifically.[39] The TAD2 complexes with p300 Taz2 and the PH domain indicated that the intrinsically disordered TAD2 can reorganize its structure, based on the residue composition, sequence, and property of the binding pocket, to maximize the native contacts with variable binding partners. The flexibility and plasticity of IDPs determine their binding specificity and affinity with variable partners in signaling pathways. Hence, the personality of the binding pocket in the folded Taz2 can determine the binding pattern of the Taz2-TAD2 complex, and the primary sequence of the disordered TAD2 can also affect the binding mode.

Single-molecule force spectroscopy,[40−42] such as atomic force microscopy (AFM) and optical tweezers, have been successfully employed to detect intermediates in the unfolding/unbinding pathways of proteins. By analyzing the recorded force curves, critical intermediate states can be identified, and the free energy landscapes can be reconstructed, which are critical to studying the kinetics and transition pathways. Our results reported here can be directly associated with force–extension curves (FECs) which are generated by repeatedly ramping up/down the applied force. By repeating unbinding/binding cycles, we would expect two types of FECs to be produced that represent the two unbinding pathways determined in our work. The FEC profile will reveal the unbinding pathways and corresponding intermediates, which can be compared with our SMD results. In addition, interpretations of FEC profiles can also benefit from the atomic-resolution structural transitions in pathways identified in the SOM analysis reported in this paper.

CONCLUSIONS

In summary, we conducted a combination of classical molecular dynamics, steered molecular dynamics, self-organizing maps, and time-resolved force distribution analysis to study the dissociation process between p300 Taz2 and p53 TAD2. Two dissociation pathways and several critical residues were determined in the unbinding process. Key residues reported here are in good agreement with previously published experimentally identified residues. Furthermore, the results show that the recognition between Taz2 and TAD2 is determined mainly by Taz2. More experimental and computational work in this field is required in the future to continue to explain the recognition mechanism of complexes involving the disordered protein.

ASSOCIATED CONTENT

Supporting Information

The Supporting Information is available free of charge at https://pubs.acs.org/doi/10.1021/jacsau.2c00358.

> MD and SMD simulation parameters, data analysis details of all 50 replicas of SMD simulations, all pre-processed simulation trajectories, and data analysis scripts available at https://unmm-my.sharepoint.com/:f:/g/personal/yihe_unm_edu/EqwwWVZFiTJCmhAXnVCCHkwBgmyDGObyy_F60RJyZKgzFQ?e=rnMbfN (PDF)

AUTHOR INFORMATION

Corresponding Authors

Stefano Motta − *Department of Earth and Environmental Sciences, University of Milano-Bicocca, Milan 20126, Italy;* ⓘ orcid.org/0000-0002-0812-6834; Email: stefano.motta@unimib.it

Yi He − *Department of Chemistry & Chemical Biology, The University of New Mexico, Albuquerque, New Mexico 87131, United States;* ⓘ orcid.org/0000-0002-6884-5312; Email: yihe@unm.edu

Authors

Tongtong Li − *Department of Chemistry & Chemical Biology, The University of New Mexico, Albuquerque, New Mexico 87131, United States*

Amy O. Stevens − *Department of Chemistry & Chemical Biology, The University of New Mexico, Albuquerque, New Mexico 87131, United States*

Shenghan Song − *Department of Chemistry & Chemical Biology, The University of New Mexico, Albuquerque, New Mexico 87131, United States*

Emily Hendrix − *Department of Chemistry & Chemical Biology, The University of New Mexico, Albuquerque, New Mexico 87131, United States*

Alessandro Pandini − *Department of Computer Science, Brunel University London, Uxbridge UB8 3PH, U.K.; The Thomas Young Centre for Theory and Simulation of Materials, London SW7 2AZ, U.K.;* orcid.org/0000-0002-4158-233X

Author Contributions

The manuscript was written through the contributions of all authors. All authors have given approval to the final version of the manuscript.

Notes

The authors declare no competing financial interest.

■ REFERENCES

(1) Vogelstein, B.; Lane, D.; Levine, J. A. Surfing p53 Network. *Nature* **2000**, *408*, 307−310.

(2) Zenz, T.; Eichhorst, B.; Busch, R.; Denzel, T.; Häbe, S.; Winkler, D.; Bühler, A.; Edelmann, J.; Bergmann, M.; Hopfinger, G.; Hensel, M.; Hallek, M.; Döhner, H.; Stilgenbauer, S. TP53 mutation and survival in chronic lymphocytic leukemia. *J. Clin. Oncol.* **2010**, *28*, 4473−4479.

(3) Rosenfeldt, M. T.; O'Prey, J.; Morton, J. P.; Nixon, C.; MacKay, G.; Mrowinska, A.; Au, A.; Rai, T. S.; Zheng, L.; Ridgway, R.; Adams, P. D.; Anderson, K. I.; Gottlieb, E.; Sansom, O. J.; Ryan, K. M. P53 status determines the role of autophagy in pancreatic tumour development. *Nature* **2013**, *504*, 296−300.

(4) Mello, S. S.; Valente, L. J.; Raj, N.; Seoane, J. A.; Flowers, B. M.; McClendon, J.; Bieging-Rolett, K. T.; Lee, J.; Ivanochko, D.; Kozak, M. M.; Chang, D. T.; Longacre, T. A.; Koong, A. C.; Arrowsmith, C. H.; Kim, S. K.; Vogel, H.; Wood, L. D.; Hruban, R. H.; Curtis, C.; Attardi, L. D. A p53 Super-tumor Suppressor Reveals a Tumor Suppressive p53-Ptpn14-Yap Axis in Pancreatic Cancer. *Cancer Cell* **2017**, *32*, 460−473.e6.

(5) Zhao, J.; Blayney, A.; Liu, X.; Gandy, L.; Jin, W.; Yan, L.; Ha, J.-H.; Canning, A. J.; Connelly, M.; Yang, C.; Liu, X.; Xiao, Y.; Cosgrove, M. S.; Solmaz, S. R.; Zhang, Y.; Ban, D.; Chen, J.; Loh, S. N.; Wang, C. EGCG binds intrinsically disordered N-terminal domain of p53 and disrupts p53-MDM2 interaction. *Nat. Commun.* **2021**, *12*, 986.

(6) Horn, H. F.; Vousden, K. H. Coping with stress: Multiple ways to activate p53. *Oncogene* **2007**, *26*, 1306−1316.

(7) Hong, H.; Takahashi, K.; Ichisaka, T.; Aoi, T.; Kanagawa, O.; Nakagawa, M.; Okita, K.; Yamanaka, S. Suppression of induced pluripotent stem cell generation by the p53-p21 pathway. *Nature* **2009**, *460*, 1132−1135.

(8) Ohtsuka, T.; Ryu, H.; Minamishima, Y. A.; Macip, S.; Sagara, J.; Nakayama, K. I.; Aaronson, S. A.; Lee, S. W. ASC is a Bax adaptor and regulates the p53-Bax mitochondrial apoptosis pathway. *Nat. Cell Biol.* **2004**, *6*, 121−128.

(9) Avantaggiati, M. L.; Ogryzko, V.; Gardner, K.; Giordano, A.; Levine, A. S.; Kelly, K. Recruitment of p300/CBP in p53-dependent signal pathways. *Cell* **1997**, *89*, 1175−1184.

(10) Lill, N. L.; Grossman, S. R.; Ginsberg, D.; DeCaprio, J.; Livingston, D. M. Binding and modulation of p53 by p300/CBP coactivators. *Nature* **1997**, *387*, 823−827.

(11) Sheahan, T., Major, V., Webb, K., Bryan, E.; Voigt, P. The TAZ2 domain of CBP/p300 directs acetylation towards H3K27 within chromatin. **2020**, bioRxiv 2020.07.21.214338.

(12) Nishimura, M.; Arimura, Y.; Nozawa, K.; Kurumizaka, H. Linker DNA and histone contributions in nucleosome binding by p53. *J. Biochem.* **2020**, *168*, 669−675.

(13) He, F.; Borcherds, W.; Song, T.; Wei, X.; Das, M.; Chen, L.; Daughdrill, G. W.; Chen, J. Interaction between p53 N terminus and core domain regulates specific and nonspecific DNA binding. *Proc. Natl. Acad. Sci. U. S. A.* **2019**, *116*, 8859−8868.

(14) Jansson, M.; Durant, S. T.; Cho, E. C.; Sheahan, S.; Edelmann, M.; Kessler, B.; La Thangue, N. B. Arginine methylation regulates the p53 response. *Nat. Cell Biol.* **2008**, *10*, 1431−1439.

(15) Teufel, D. P.; Freund, S. M.; Bycroft, M.; Fersht, A. R. Four domains of p300 each bind tightly to a sequence spanning both transactivation subdomains of p53. *Proc. Natl. Acad. Sci. U. S. A.* **2007**, *104*, 7009−7014.

(16) Jenkins, L. M. M.; Feng, H.; Durell, S. R.; Tagad, H. D.; Mazur, S. J. Characterization of the p300 Taz2-p53 TAD2 complex and comparison with the p300 Taz2-p53 TAD1 complex. *Biochemistry* **2015**, *54*, 2001−2010.

(17) Arai, M.; Ferreon, J. C.; Wright, P. E. Quantitative analysis of multisite protein-ligand interactions by NMR: Binding of intrinsically disordered p53 transactivation subdomains with the TAZ2 domain of CBP. *J. Am. Chem. Soc.* **2012**, *134*, 3792−3803.

(18) Ithuralde, R. E.; Turjanski, A. G. Phosphorylation regulates the bound structure of an intrinsically disordered protein: The p53-TAZ2 case. *PLoS One* **2016**, *11*, No. e0144284.

(19) Feng, H.; Jenkins, L. M. M.; Durell, S. R.; Hayashi, R.; Mazur, S. J.; Cherry, S.; Tropea, J. E.; Miller, M.; Wlodawer, A.; Appella, E.; Bai, Y. Structural Basis for p300 Taz2-p53 TAD1 Binding and Modulation by Phosphorylation. *Structure* **2009**, *17*, 202−210.

(20) Åberg, E.; Karlsson, O. A.; Andersson, E.; Jemth, P. Binding Kinetics of the Intrinsically Disordered p53 Family Transactivation Domains and MDM2. *J. Phys. Chem. B* **2018**, *122*, 6899−6905.

(21) Huang, J.; Rauscher, S.; Nawrocki, G.; Ran, T.; Feig, M.; de Groot, B. L.; Grubmüller, H.; MacKerell, A. D. CHARMM36m: An improved force field for folded and intrinsically disordered proteins. *Nat. Methods* **2016**, *14*, 71−73.

(22) Motta, S.; Pandini, A.; Fornili, A.; Bonati, L. Reconstruction of ARNT PAS-B Unfolding Pathways by Steered Molecular Dynamics and Artificial Neural Networks. *J. Chem. Theory Comput.* **2021**, *17*, 2080−2089.

(23) Motta, S.; Callea, L.; Bonati, L.; Pandini, A. PathDetect-SOM: A Neural Network Approach for the Identification of Pathways in Ligand Binding Simulations. *J. Chem. Theory Comput.* **2022**, *18*, 1957−1968.

(24) Kaski, S.; Kangas, J.; Kohonen, T. Bibliography of self-organizing map (SOM) papers: 1981−1997. *Neural Comput. Surv.* **1998**, *1*, 1−176.

(25) Oja, M.; Kaski, S.; Kohonen, T. Bibliography of self-organizing map (SOM) papers: 1998−2001 addendum. *Neural Comput. Surv.* **2003**, *3*, 1−156.

(26) Miljković, D. Brief review of self-organizing maps. *2017 40th International Convention on Information and Communication Technology, Electronics and Microelectronics (MIPRO)*; IEEE, 2017; Vol. 1061−1066.

(27) Costescu, B. I.; Gräter, F. Time-resolved force distribution analysis. *BMC Biophys.* **2013**, *6*, 5.

(28) Wojciak, J. M.; Martinez-Yamout, M. A.; Dyson, H. J.; Wright, P. E. Structural basis for recruitment of CBP/p300 coactivators by STAT1 and STAT2 transactivation domains. *EMBO J.* **2009**, *28*, 948−958.

(29) Ferreon, J. C.; Martinez-Yamout, M. A.; Dyson, H. J.; Wright, P. E. Structural basis for subversion of cellular control mechanisms by the adenoviral E1A oncoprotein. *Proc. Natl. Acad. Sci. U. S. A.* **2009**, *106*, 13260−13265.

(30) Krois, A. S.; Ferreon, J. C.; Martinez-Yamout, M. A.; Dyson, H. J.; Wright, P. E. Recognition of the disordered p53 transactivation domain by the transcriptional adapter zinc finger domains of CREB-binding protein. *Proc. Natl. Acad. Sci. U. S. A.* **2016**, *113*, E1853−E1862.

(31) Krauskopf, K.; Gebel, J.; Kazemi, S.; Tuppi, M.; Löhr, F.; Schäfer, B.; Koch, J.; Güntert, P.; Dötsch, V.; Kehrloesser, S. Regulation of the Activity in the p53 Family Depends on the Organization of the Transactivation Domain. *Structure* **2018**, *26*, 1091−1100.e4.

(32) Li, T.; Stevens, A. O.; Gil Pineda, L. I.; Song, S.; Ameyaw Baah, C. A.; He, Y. Changes in structure and flexibility of p53 TAD2 upon binding to p300 Taz2. *J. Theor. Comput. Chem.* **2020**, *19*, 2040007.

(33) McGibbon, R. T.; Beauchamp, K. A.; Harrigan, M. P.; Klein, C.; Swails, J. M.; Hernández, C. X.; Schwantes, C. R.; Wang, L.-P.; Lane, T. J.; Pande, V. S. MDTraj: A Modern Open Library for the Analysis of Molecular Dynamics Trajectories. *Biophys. J.* **2015**, *109*, 1528−1532.

(34) Skjærven, L.; Jariwala, S.; Yao, X.-Q.; Grant, B. J. Online interactive analysis of protein structure ensembles with Bio3D-web. *Bioinformatics* **2016**, *32*, 3510−3512.

(35) Grant, B. J.; Rodrigues, A. P. C.; ElSawy, K. M.; McCammon, J. A.; Caves, L. S. D. Bio3d: an R package for the comparative analysis of protein structures. *Bioinformatics* **2006**, *22*, 2695−2696.

(36) Skjærven, L.; Yao, X.-Q.; Scarabelli, G.; Grant, B. J. Integrating protein structural dynamics and evolutionary analysis with Bio3D. *BMC Bioinf.* **2014**, *15*, 399.

(37) Grant, B. J.; Skjærven, L.; Yao, X. Q. The Bio3D packages for structural bioinformatics. *Protein Sci.* **2021**, *30*, 20−30.

(38) Shoemaker, B. A.; Portman, J. J.; Wolynes, P. G. Speeding molecular recognition by using the folding funnel: The fly-casting mechanism. *Proc. Natl. Acad. Sci. U. S. A.* **2000**, *97*, 8868−8873.

(39) Okuda, M.; Nishimura, Y. Extended string binding mode of the phosphorylated transactivation domain of tumor suppressor p53. *J. Am. Chem. Soc.* **2014**, *136*, 14143−14152.

(40) Marszalek, P. E.; Lu, H.; Li, H.; Carrion-Vazquez, M.; Oberhauser, A. F.; Schulten, K.; Fernandez, J. M. Mechanical unfolding intermediates in titin modules. *Nature* **1999**, *402*, 100−103.

(41) Liphardt, J.; Onoa, B.; Smith, S. B.; Tinoco, I. J.; Bustamante, C. Reversible unfolding of single RNA molecules by mechanical force. *Science* **2001**, *292*, 733−737.

(42) Cecconi, G.; Shank, E. A.; Bustamante, C.; Marqusee, S. Biochemistry: Direct observation of the three-state folding of a single protein molecule. *Science* **2005**, *309*, 2057−2060.